Centrifuge Model Test at Zhejiang University for LEAP-ASIA-2018

Qiang Ma[1], Yan-Guo Zhou[1]*, Kai Liu[1], Yun-Min Chen[1]

Abstract:

Two centrifuge models with the same relative density were conducted in different centrifugal acceleration (30 g for Model-A and 15 g for Model-B) at Zhejiang University to validate generalized scaling law in LEAP-ASIA-2018. The same model used in LEAP-UCD-2017 representing a 5-degree slope consisting of saturated Ottawa F-65 was repeated. The bending disk was installed to check the degree of saturation and the temperature-fluid viscosity curves also measured in the experiment. This paper describes the facilities, test procedures, and the response of acceleration, excess pore water pressures and displacement etc. Uncertainty analysis is also carried out in input parameters (e.g. achieved PGA, achieved density and the degree of saturation). Preliminary ZJU experiment results show that the generalized scaling law is applicable to the acceleration response while a weak applicability to displacement response.

[1]Institute of Geotechnical Engineering, MOE Key Laboratory of Soft Soils and Geoenviromental Engineering, Center for Hypergravity Experimental and Interdisciplinary Research, Zhejiang University, P. R. China
* Corresponding author, Ph.D., Professor, E-mail: qzking@zju.edu.cn

1. Introduction

LEAP (Liquefaction Experiments and Analysis Project) is an international effort, which aimed to provide a set of high quality laboratory and centrifuge test data to assess the capabilities of constitutive and numerical models (e.g. Kutter et al. 2015, Manzari et al. 2015). The results of LEAP-Kyoto-2013 and 2014 showed some inconsistency between different centrifuge tests due to the differences of laminar containers, which caused challenges for numerical simulations (Tobita et al. 2015). Therefore, rigid boxes were adopted in LEAP-GWU-2015 to avoid the numerical modeling complexities associated with the special boundary conditions created by different types of laminar containers. Several numerical simulations also conducted in LEAP-GWU-2015, showing great consistencies with experimental tests. Kutter et al. (2015) compared the results from different centrifuge facilities and found larger differences than ideal due to variability of input parameters (i.e., density, fabric, saturation etc.). In summary of LEAP-GWU-2015, Kutter et al. (2017) suggested that more rigorous site investigation should be used to determine the density and saturation of the soils (such as in-fight CPT testing). New methods such as high-speed cameras with PIV analysis are also recommended to for tracing dynamic surface lateral displacement. Thus, better practical experimental technology and measuring techniques were adopted in LEAP-UCD-2017, including in-fight CPT testing for estimating soil density, high-speed camera for tracing marker displacement as well as shear-wave velocity for detecting initial state of the model (Zhou et al. 2017).

In LEAP-ASIA-2018, two centrifuge models were conducted at Zhejiang University to validate generalized scaling law. Large geotechnical centrifuge ZJU-400, uniaxial hydraulic shaker and advanced in-flight Bender Element (BE) system, other unique techniques, including a two-dimensional in-flight miniature CPT system, Bending Disk system (BD) and high-speed camera were also used in Zhejiang University in LEAP-ASIA-2018. Zhejiang University rigorously followed the specifications and procedures and gained reliable results. The achieved density of two models are closed to the target and the achieved Sr > 99.5%. The input motion was well controlled and the effective PBA matched the target one. This paper describes the facilities and test procedures, uncertainty analysis is carried out in input parameters and some preliminary experimental results are discussed as well, which is contribute to further researchers to understand the experimental benchmark data of Zhejiang University in LEAP-ASIA-2018.

2. Test Facilities and Specifications

2.1 Test facilities

The LEAP-ASIA-2018 tests of Zhejiang University were performed by using the ZJU-400 centrifuge with in-fight uniaxial shaker and bender element (BE)/bending disk (BD) testing system, which was detailed introduced in Zhou et al. (2017).

The same rigid model container was used as LEAP-UCD-2017, which had the inner dimension of 770 mm long, 400 mm wide and 500 mm deep. The container was shortened to 666 mm in length to match the prototype specification of 20 m in length. The supporting blocks are 52 mm thick aluminum plate, which is braced at six locations and bolted to the end walls of the container, illustrated in Figure 1. The blocks are well sealed to prevent drainage along the aluminum container interfaces.

A two-dimensional miniature CPT system used in LEAP-UCD-2017 was applied to evaluate the uniformity and density of the soil models before each destructive motion. The CPT system includes the cone penetrometer with a cone tip 6 mm in diameter and apex angle of 60° (Liu et al., 2018).

2.2 Model Geometry and Instrumentation Layout

In prototype, the models conducted in LEAP-ASIA-2018 represents a 5-degree, 4 m deep at midpoint, 20 m long sand slope deposit of Ottawa F-65. The soil surface normal to slope direction was not curved according to the radius of the centrifuge because the shaking direction is parallel to the axis of the centrifuge.

Figure 1 illustrated the instrumentation locations in the model. There were 4 horizontal accelerometers (AH1-AH4) and 4 pore pressure transducers located at the midpoint along the shaking direction to minimize the boundary effects from the rigid walls. Two additional accelerometers (AH11 and AH12) were attached on the bottom of container to record the achieved base motion. Two vertical accelerometers were installed at the top of the container to monitor vertical and rocking accelerations. Another 4 horizontal accelerometers and 2 pore pressure transducers (AH6, AH7, AH9 and AH10; P6, P8-P10) were included at equivalent depths as sensors in the central array and were intended to help in understanding the effect of the container boundaries on the model response. Three pairs of bender elements, at the depth of 1 m, 2 m, and 3 m respectively, were placed to measure vertically polarized and horizontal travelling SV shear-wave velocity. A pare of bending disks were also installed to measure P-wave velocity after model saturation.

Surface markers were placed on the surface of the soil to trace the deformation during soil liquefaction. The specified surface markers were red shown in Figure 2, which made by a 10 mm length, 25 mm in diameter PVC tube with an aluminum cross bar fixed in center. The black surface markers made of zip ties were also employed and all the surface markers were installed in a 50 mm×50 mm grid (model scale). 12 colored (blue) sand columns were used to curve lateral spreading profile by excavation after the final spin down.

Five high-speed cameras (GoPro cameras) were installed on the camera frame to record the lateral displacement of surface markers on different regions of the model during spinning. The finished model photographed in Figure 2.

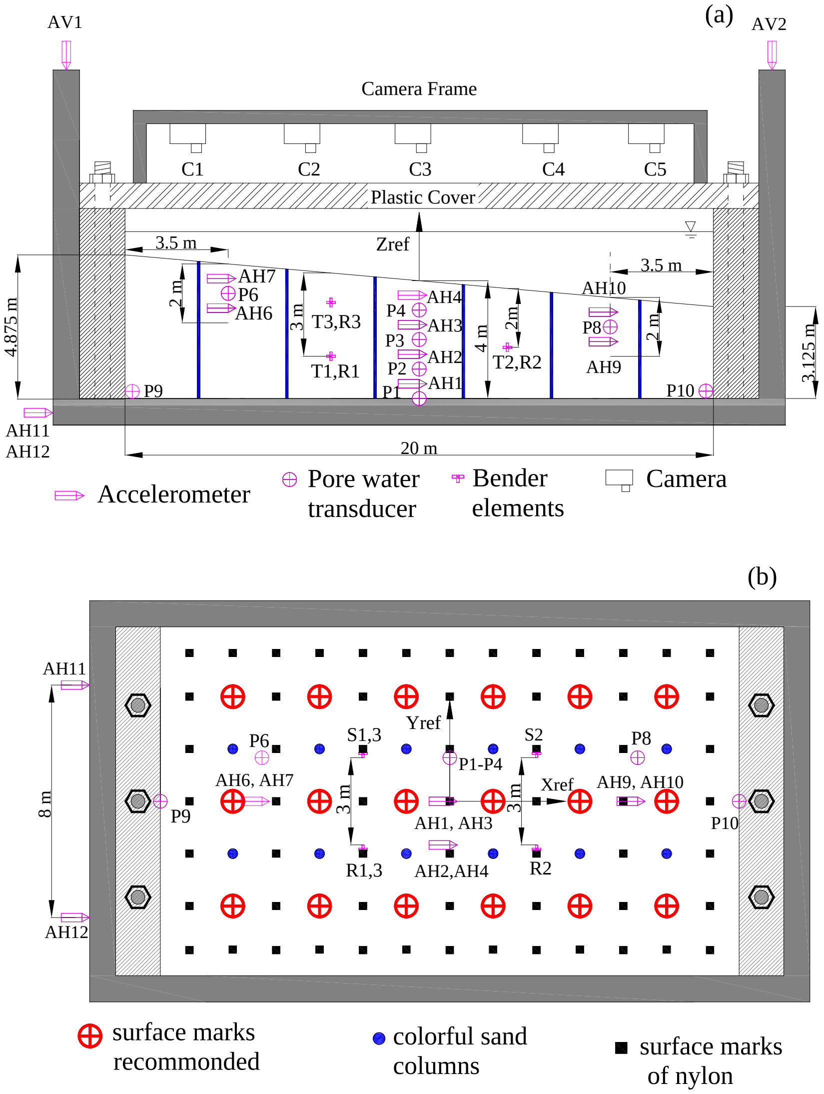

Figure 1: Model geometry and instrumentation layout (prototype scale)
(a)Side view (b) Top view

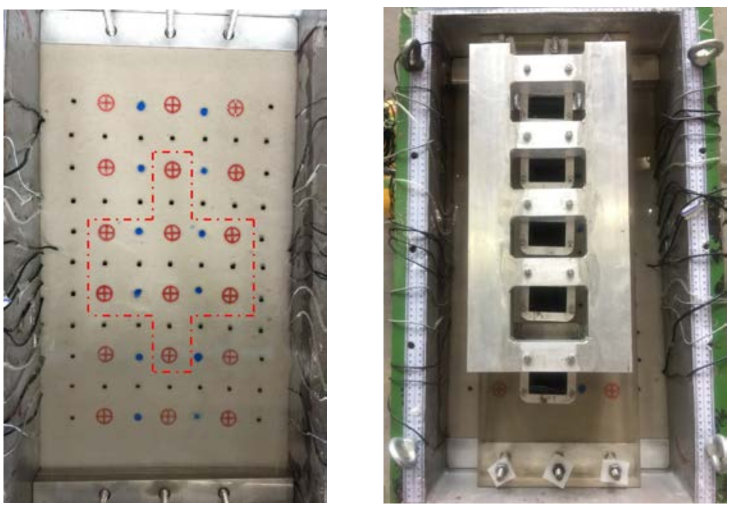

(a) (b)

Figure 2: Photograph of finished model
(a) Surface marker and colored sand columns (b) High-speed cameras

3. Model Preparation

3.1 Test Material

The same Ottawa F-65 sand was used as the LEAP-UCD-2017, the grain size distribution curve, physical properties and additional material properties of Ottawa F-65 sand, including triaxial, simple shear, and permeability test data, could be found in Carey et al. (2016).

3.2 Scaling Law

One purpose of LEAP-ASIA-2018 is the verification of the generalized scaling law. The generalized scaling law (GSL) was applied in the experiment consequently, which contains two stages. In the first stage, the prototype is scaled down into a virtual model using a 1 g filed scaling law with a scaling factor μ. In the second stage, the virtual model is scaled down into the physical model applying the conventional centrifuge scaling law with a scaling factor η. More detailed description of GSL could reference Iai and Tobita (2009). Two models were conducted at ZJU-400 centrifuge, called Model-A and Model-B respectively. The generalized scaling factors were listed in Table 1.

3.3 Model Preparation and Saturation

Air pluviation method was adopted to ensure a high level of uniformity when prepare the model. The calibration was implemented before pluviating the model. The target density is ρ_d = 1.654 g/cm^3, the estimated final achieved density detailed in Table 2. The achieved density was slight loose than the target.

Table 1: Generalized scaling factors implemented in ZJU experiment

	Scaling Factors (prototype/model)		
	GSL	Model-A	Model-B
1g	μ	1	2
centrifuge	η	30	15
Length	$\mu\ \eta$	30	30
Time	$\mu^{0.75}\ \eta$	30	25.2
Frequency	$\mu^{-0.75}\ \eta^{-1}$	1/30	1/25.2
Acceleration	$1/\ \eta$	1/30	1/15
Displacement	$\mu^{1.5}\ \eta$	30	42.4
Stress	μ	30	15
Strain	$\mu^{0.5}$	1	1.4
Permeability	$\mu^{0.75}\ \eta$	30	25.2
Pore pressure	μ	30	15

Table 2: Achieved density for each model

Model	Mass of sand	Volume after saturation	Average density ρ_d
	g	cm^3	g/cm^3
Model-A	59098	36376.8	1.625
Model-B	60103	36812.4	1.633

Silicone oil with density of 0.95 g/cm^3 (25℃) and 30 times of viscosity of water for Model-A and 25.2 times for Model-B was used as pore fluid to overcome the confliction of time scaling factors. Temperature-fluid viscosity curves obtained before saturation by using a MCR302 rotational rheometer (manufacturer: Anton Paar). The testing results illustrated in Figure 3. Owing to the spin of centrifuge, the temperature of silicone oil commonly changed between 24 to 28 ℃ for Model-A and 27 to 30 ℃ for Model-B during the test, which would cause about 4.6% and 9.6% decrease of viscosity.

When saturation, the oil tank and model container were kept under the same vacuum level (around 85 kPa) and the oil was firstly de-aired more than 24 hours. Then transport silicone oil from the reservoir to the container was driven by gravity feed. The saturation speed was controlled to prevent soil disturbance at the bottom of container. When saturation was accomplished, bending disk testing system was used to check the degree of saturation. Figure 4 represents the typical BD test result, the measured V_p around 1075 m/s. According to Zhou et al. (2017), the achieved Sr > 99.5%.

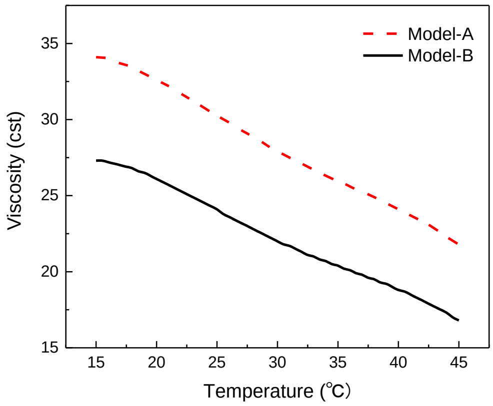

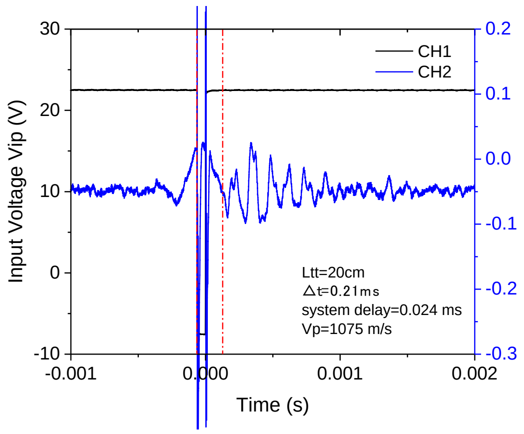

Figure 3: Temperature-fluid viscosity curve **Figure 4:** Typical signal of BD test

3.4 Motion Sequence

The input base acceleration for each model consisted a sequence of 3 destructive motions with the same maximum acceleration of 0.25 g (prototype scale). All motions represented 1 Hz ramped sine wave with 16 cycle, shown in Figure 5.

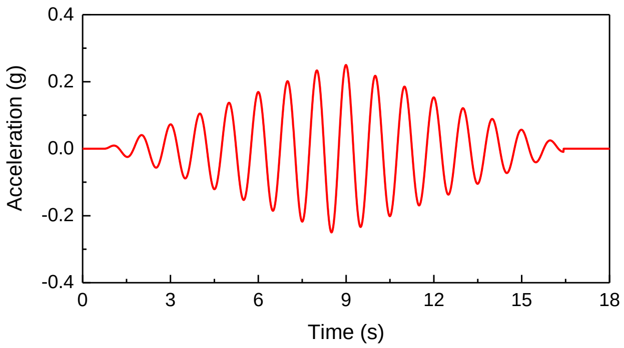

Figure 5: Ground motion sequence for each motion

4. Test Procedure and Achieved Motions

4.1 Test Procedure

The test procedure is shown in Table 3. Before the centrifuge spin up, a careful survey of the surface markers was carried out and the temperature of silicone oil was measured. Then the centrifuge was spun up to 10 g, 20 g and 30 g step by step (7.5g and 15g for Model-B). when the pore pressure was stable at each g-level, the shear wave velocity was measured by using BE testing system. After reaching the target centrifugal acceleration, the model then was subjected to a non-destructive step wave, which is used to characterize the model. The CPT test was carried out to determine the density of the model before each destructive motion. After that, a destructive motion (shown in Figure 5) was executed and then, another step wave conducted when the excess pore pressure was fully dissipated. The centrifuge was spun down step by step and V_s was measured at each step after all the above procedures accomplished. Finally, surface markers and temperature were measured. Each model and each motion followed the same procedure except Model-B second motion missing the step wave after destructive motion.

Table 3: Test procedure and events of interest in each motion

No.	Name	N(g	Description	No.	Name	N(g)	Description
1	S-1	1	Surface marker	9	B	30	Destructive motion
2	BE-1	1	Vs measurement	10	BE-5	30	Vs measurement
3	A		Swing up	11	SW-2	30	Step-wave
4	BE-2	10	Vs measurement	12	C		Start of swing down
5	BE-3	20	Vs measurement	13	BE-6	20	Vs measurement
6	BE-4	30	Vs measurement	14	BE-7	10	Vs measurement
7	SW-1	30	Step-wave	15	BE-8	1	Vs measurement
8	CPT-1	30	CPT test	16	S-2	1	Surface marker

4.2 In-flight Measurement

CPT test was conducted in 30 g for Model-A and 15 g for Model-B with the velocity of penetration 0.6 mm per second and sample rate 1Hz. One of the key parameters controlling tip resistance is effective stress (Jamiolkowski et al., 1985), so dimensional analysis was adopted to eliminate the influence of stress caused by different centrifugal acceleration. Figure 6 demonstrates the normalized tip resistance (defined in Eq.1) versus normalized depth (defined in Eq.2) for two models.

$$Q = \frac{q_c}{\sqrt{\sigma_v^{'} p_a}} \qquad \text{Eq.1}$$

$$Z = \frac{z}{B} \qquad \text{Eq.2}$$

Where q_c and σ_v' is tip resistance and vertical effective stress, expressed in MPa, p_a is atmospheric pressure, 101 kPa; z is penetration depth, B is cone diameter, 6 mm.

The normalized resistance nearly linearly increased, which indicates the uniformity of both two models. According to Kim et al (2015), the slope of the curve represents the relative density of sand. The result indicated that Model-A and Model-B have a closed density, which agreed with table 3 results.

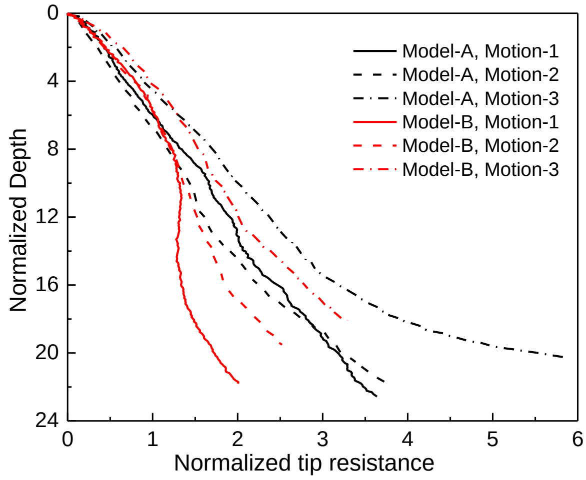

Figure 6: Normalized cone tip resistance

There pair of bender elements (BE) were used to measure the V_s of model. Figure 7 (a) gives a typical signal of BE during spinning, indicating the arrival of receiver is well distinguishable to ensure the reliability of BE results. Figure 7 (b) shows the fitted Hardin curve, the G_{max} was calculated through different g-level BE results.

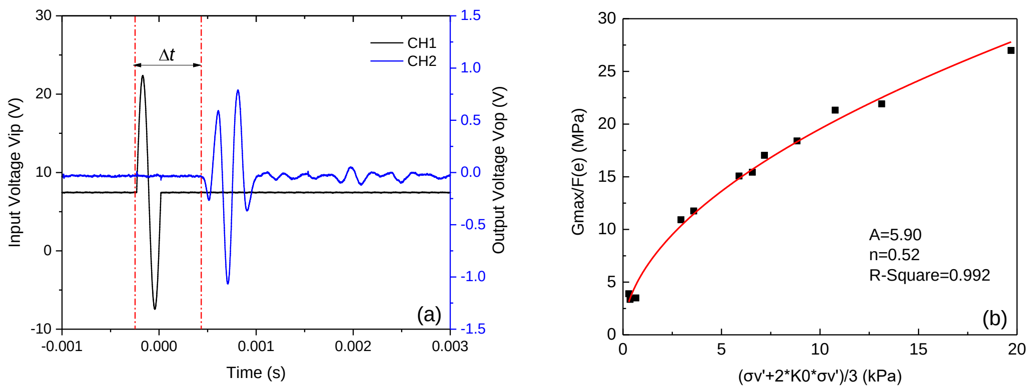

Figure 7: (a) Typical signal of BE (b) Hardin curve gained from BE test

As shown in Figure 1(a), five high-speed GoPro cameras were installed above the slope surface to record movement of surface markers during the destructive motion. The videos were converted to displacement time history by Geo-PIV analysis procedure (e.g. White et al. 2003). Five points located at different region of the surface marker were analyzed to ensure reliable results shown in Figure 8 (a). The Figure 8(b) demonstrates typical results of dynamic displacement of one surface marker from five points, showing high consistency within five points. The residual displacement value obtained using videos are agreed with that measured by hand afterwards.

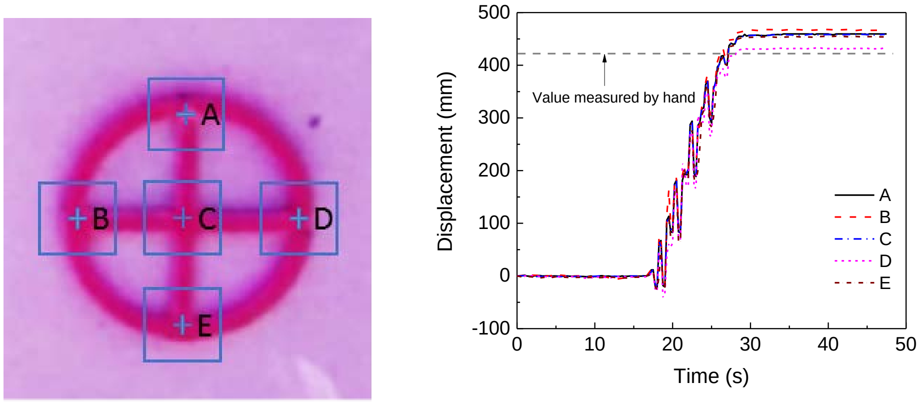

(a) (b)

Figure 8: (a) PIV points on surface marker; (b) Typical result from PIV

4.3 Achieved Motions

In dynamic centrifuge testing, it is crucial to impose acceleration to models which is as close as possible to the target acceleration. Assessment of the similarities and differences between achieved input and target motions is fundamental to address the LEAP validation objectives. The concept of effective PGA was adopted to evaluate the accuracy and efficiency of the motions. The effective PGA is defined as below:

$$\mathrm{PGA}_{effective} = \mathrm{PGA}_{1Hz} + 0.5 \times \mathrm{PGA}_{hf} \quad \text{Eq.3}$$

In which PGA_{hf} represents the peak acceleration of the high frequency component of the motion, $\mathrm{PGA}_{1\mathrm{Hz}}$ denotes the peak acceleration which was isolated by use of a notched band pass filter with corner frequencies of 0.9 and 1.1 Hz. The results of all the input motions for two models are summarized in Table 4. It is found that $\mathrm{PGA}_{1\mathrm{Hz}}$ values of AH11 are smaller than AH12 for Model-A, while almost the same between AH11 and AH12 for Model-B, indicating that there was a small angle between AH11 and motion direction in Model-A.

Figure 9 (a) and (b) compares the achieved and target acceleration time histories and velocity histories for Model-A three motions, the velocity time series obtained by integrating acceleration. The achieved PBA usually 10-20% higher than target PBA, while the achieved PBV only about 90% of target one, which is because the achieved motion contained high frequency components. 5% damped acceleration response spectra (ARS) for model-A three motions is shown in Figure 9 (c), the average achieved peak spectral acceleration at T = 1 s is 1.5 g, lower than target one (approximately 1.9 g). Figure 9 (c) also indicates that the achieved motion contained some higher frequency components especially in 3Hz and 5Hz.

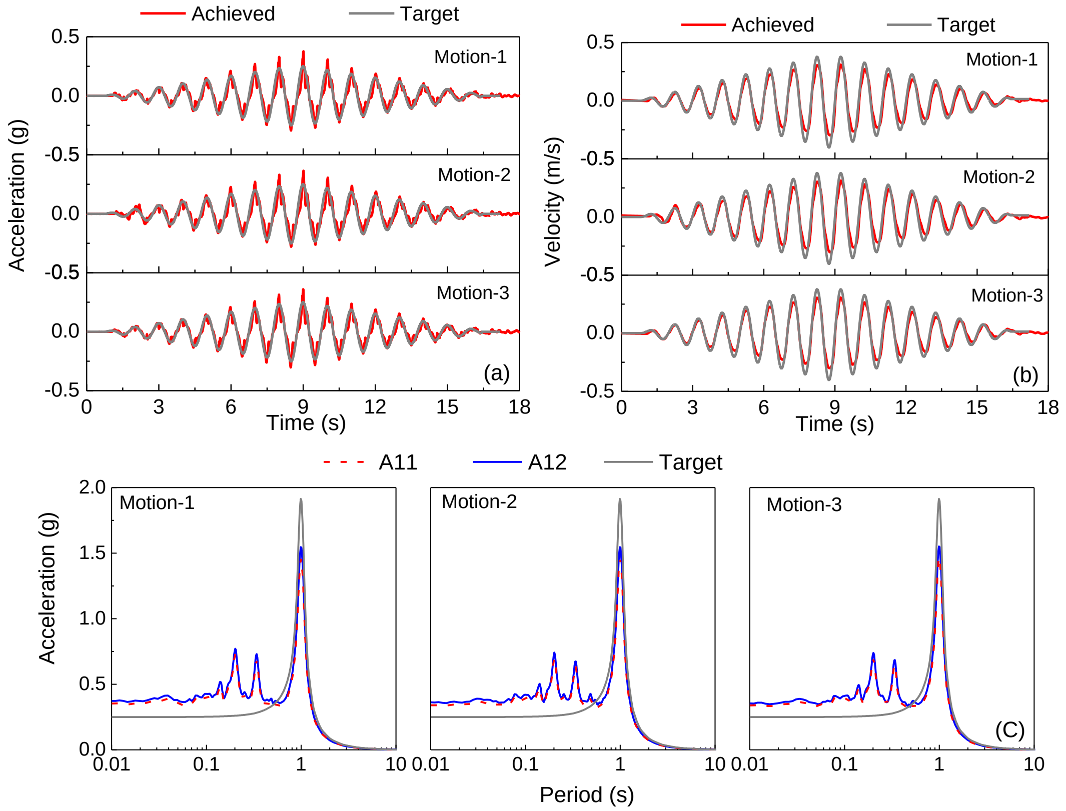

Figure 9: Comparation between target and achieved motions of Model-A
(a) Acceleration time history (b) Velocity time history
(c) Acceleration response spectra

Table 4: Ground motion sequence for LEAP-ASIA-2018experiments (unit: g)

Model	Motion	Accelerometer	PBA_{tar}	PBA_{1Hz}	PBA_{hf}	PBA_{ach}	PBA_{eff}
A	1	A11	0.25	0.184	0.171	0.354	0.270
		A12		0.195	0.18	0.374	0.285
	2	A11	0.25	0.184	0.157	0.341	0.263
		A12		0.195	0.169	0.363	0.280
	3	A11	0.25	0.186	0.154	0.339	0.263
		A12		0.196	0.16	0.355	0.276
B	1	A11	0.25	0.205	0.147	0.347	0.279
		A12		0.204	0.146	0.345	0.277
	2	A11	0.25	0.199	0.154	0.344	0.276
		A12		0.198	0.15	0.339	0.273
	3	A11	0.25	0.197	0.139	0.33	0.267
		A12		0.199	0.138	0.328	0.268

For length limit, Figure 10 only gives information about the measured vertical motions for Model-A, Motion-1. The grey lines indicate the unfiltered motions, and the black lines are band-pass filtered the components of the motion between 0.3 and 3 Hz. Although zero vertical acceleration is expected during shaking, the hydraulic shaker produced unintended vertical component in addition to the desired horizontal accelerations. Besides, Coriolis acceleration will also contribute to the measured vertical acceleration. Little phase shift between AV1 and AV2 is observed from Figure 10, revealing that the container was a negligible rocking during shaking.

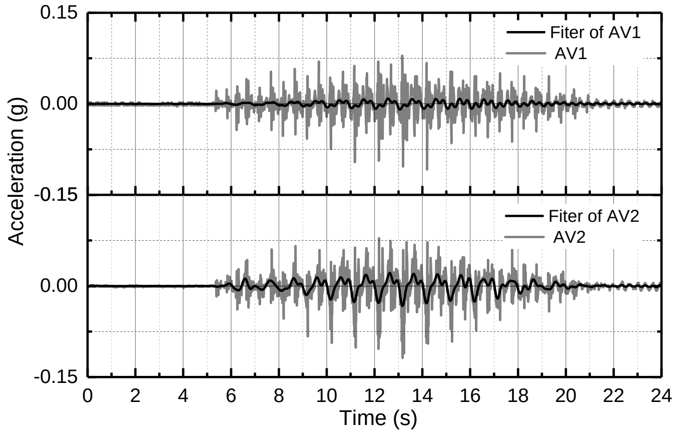

Figure 10: Vertical accelerations on container ends

5. Test Results

5.1 Acceleration Responses

Figure 11 (a) only shows typical acceleration time histories of Motion-1 in Model-A due to length restriction, other results in ZJU experiments are similar with the instance. The acceleration time histories show de-amplification in upslope direction and significant negative dilation spikes in downslope direction for AH1-AH4, which have been observed in LEAP-GWU-2015 and LEAP-UCD-2017(e.g. Carey et al. 2017). The spikes tend to be most exaggerated near the slope surface where the soil easily dilated. When the sharp spikes occurred, the waveform significantly changes both in frequency and amplitude from the base motion. Figure 11 (b) demonstrates the Fourier spectrum, some higher frequency occurred owing to dilation of soil.

Figure 12 contrasts the central array acceleration response of Motion-1. The two models time histories of acceleration show a high consistency not only in trends but also in value, which reveals that GSL is applicable to acceleration response in the experiments.

5.2 Pore Pressure Response

Figure 13 compares the central vertical array of time histories of excess pore pressure ratio r_u ($\Delta u/\sigma_v$') for Motion-1 in Model-A and Model-B. P1, P2, P3, and P4 were specified to be at depths of 1, 2, 3, and 4 m respectively, and the initial vertical effective stresses are approximately 10, 20, 30, and 40 kPa respectively. The results show a good agreement trance with Model-A and Model-B, indicating the promising applicability of GSL. Severe liquefaction was occurred and significant dilation spikes were observed for all transducers for the motion is strong enough to liquefied the slope from top to the bottom. The deeper sensors take longer to reach liquefied and excess pore pressure dissipated almost immediately after motion, while the shallow one P4 liquefied firstly attained r_u =1 and lasted about 15 s after motion because pore water drains upward toward the upper transducers.

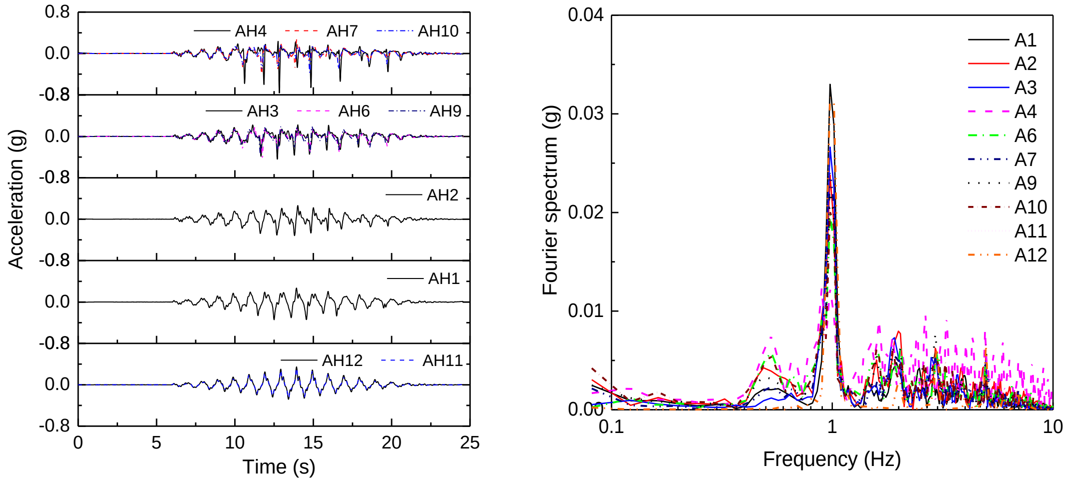

(a) (b)

Figure 11: Acceleration response of Model-A, Motion-1
(a) Time histories (b) Fourier spectrum

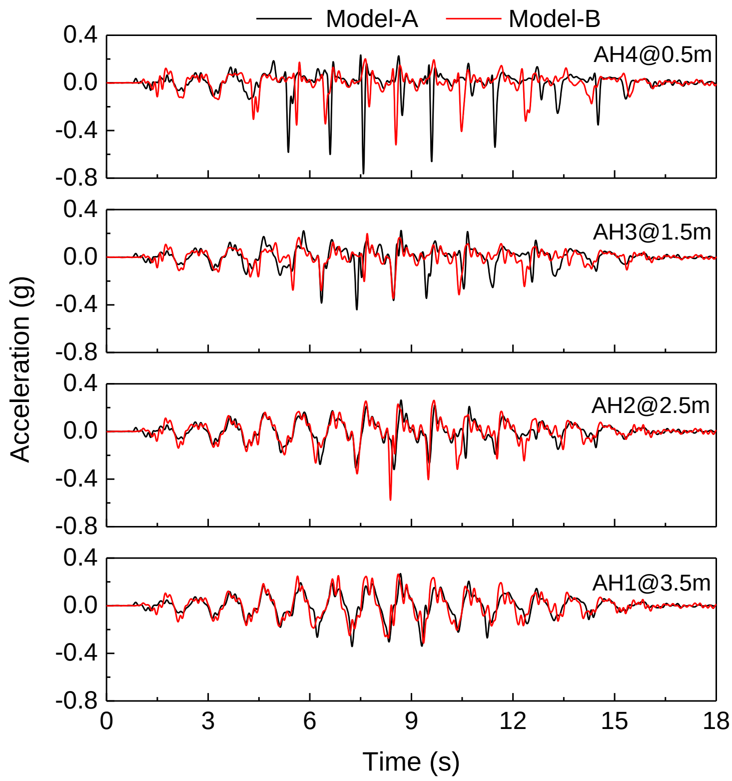

Figure 12: Acceleration response between Model-A and B, Motion-1

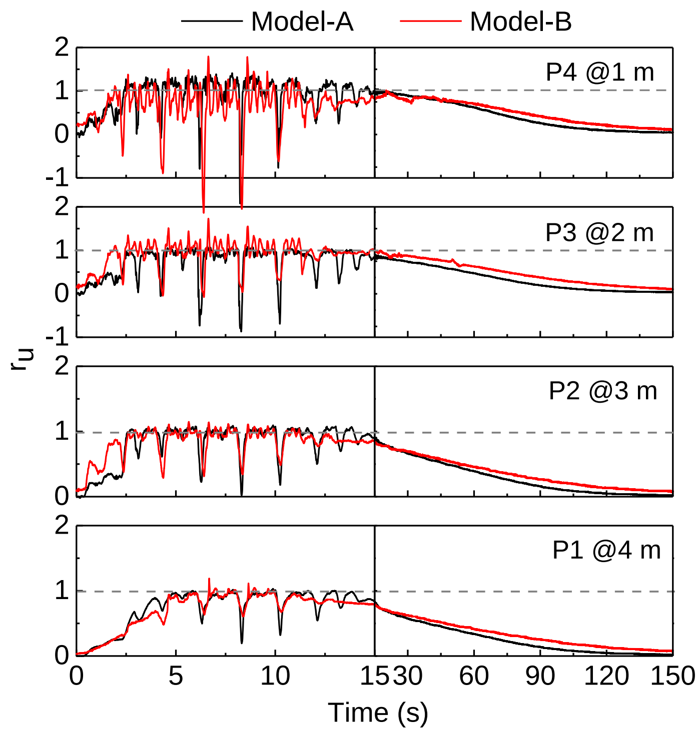

Figure 13: Pore pressure time history: Motion-1

5.3 Displacement Response

5.3.1 Vertical Displacement

For all experiments, similar trends are observed that the soil surface settles at the top of the slope higher than toe. A typical result (Model-A) shown in Figure 14. Significant settlement at the top of the slop was occurred during the first motion while heave was observed in the toe. Then the settlement decreased with the number of motions dramatically for the destructive motions densified the soil. Noticing that Motion-3 nearly had a uniform settlement along the slope, no apparent heave at toe of the slope.

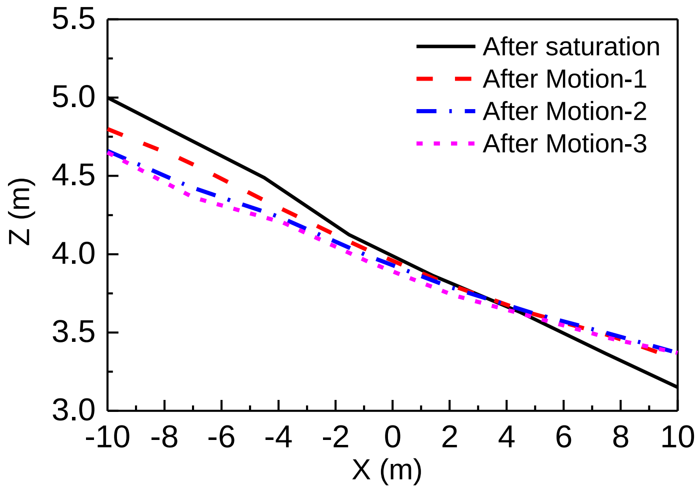

Figure 14: The development of surface settlement (Model-A)

5.3.2 Horizontal Displacement Response

Table 5 lists the average horizontal displacement D_h and standard deviation of vertical displacement σ for each motion, which calculated from only red surface marker which located in red dotted line frame shown in Figure 2 (a). Compared the average horizontal displacement of Model-A and B for each motion, some discrepancies were observed. The horizontal displacement of Model-A larger than Model-B during the Motion-2 and 3, whereas significantly smaller in Motion-1. Standard deviation of Model-B larger than Model-A indicating more scatter for Model-B. The scaling factor of displacement in the GSL is much larger for Model-B than A, any little measurement error would be amplified significantly and scattered the data. Thence, special care had to be taken in measurement of ground displacement when applied the GSL.

The lateral displacement profiles in Figure 15 were obtained from excavation of colored sand columns. The profiles show that the displacement distributed over the whole depth and reached maximum at the surface. Consistent with the observation of surface spreading, the lateral displacements near the side walls were also smaller than those at the mid-slope.

Table 5: Average values of lateral displacement after each motion (unit: mm)

Model	Motion-1		Motion-2		Motion-3	
	D_h	σ	D_h	σ	D_h	σ
A	393.75	30.70	187.50	30.00	110.63	37.45
B	593.97	114.73	137.89	47.43	45.08	16.56

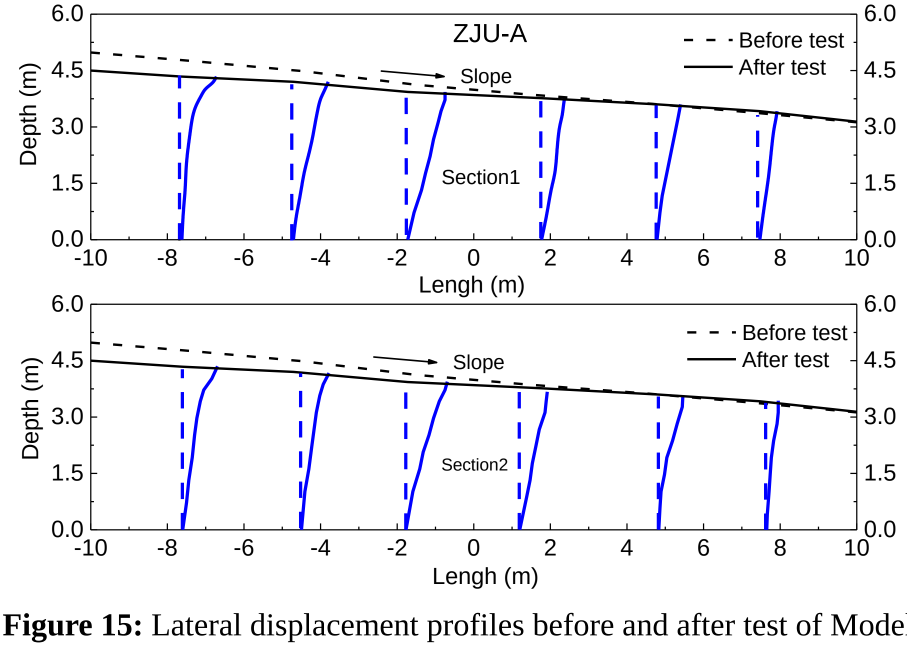

Figure 15: Lateral displacement profiles before and after test of Model-A

6. Summary and Conclusion

Two centrifuge tests were conducted at Zhejiang University in LEAP-ASIA-2018 which were designed in the same target densities and subjected the same three motions under centrifugal acceleration of 30 g and 15 g respectively. Generalized scaling law was applied in the tests to verify the application of the GSL. In this paper information on test facilities, model setup and preparation, test procedures, in-fight characterizations and analysis of the achieved motion and tests results is presented.

The facilities adopted in LEAP-ASIA-2018 was the same as LEAP-UCD-2017. Besides the bending disk system was carried out to evaluate the degree of saturation. MCR302 rotational rheometer was used to gain temperature-fluid viscosity curve of silicone oil. The decrease of viscosity caused by the rise of temperature was also evaluated.

The achieved densities in both models were a bit loose than target one. The CPT results indicated that two models had a closed density. The achieved PBA usually 10-20% higher than target PBA, while the achieved PBV only about 90% of target one. The achieved effective PGA for each motion roughly matches the targets. ARS shows the achieved motions were smaller than the target of 1Hz components and some high frequency components were observed in input motion. The vertical accelerations at opposite ends of container were small, indicating a negligible rocking effect during shaking.

Typical results are exampled to explain the response of two models. Liquefaction was occurred in the whole slope. Both of two models had similar acceleration response and pore water response. Spikes due to dilatancy were observed in acceleration time history, which are consistent with drops in excess pore pressure. The speed of dissipation is also close for two models. Lateral and vertical displacements for each motion were surveyed via some surface markers, which show a similar trend but different in value.

The above results show a promising applicability of GSL especially in modelling larger-scale prototype. However, the scaling factor of displacement in the GSL is much bigger than conventional scaling law if a large μ was adopted. Any little measurement error would be amplified significantly. So, special care had to be taken in measurement of ground displacement when usage of GSL.

7. Acknowledgements

This study is supported by the National Natural Science Foundation of China (Nos. 51578501, 51778573) and the Major Science and Technology Projects of Zhejiang Province "Centrifugal Hypergravity and Interdisciplinary Experiment Facility". The authors would thank Mr. Zizhuang Yan, Mr. Jinshu Huang of Zhejiang University for their great help during the centrifuge model tests.

8. References

Carey TJ, Kutter B.L., Manzari M.T., Zeghal M., Vasko, A. (2016). LEAP soil properties and element test data, http://doi.org/10.17603/DS2WC7W.

Carey, T.J., Hashimoto, T., Cimin, D., Kutter, B.L. (2017). LEAP-GWU-2015 Centrifuge Test at UC Davis. Soil Dynamics and Earthquake Engineering, https://doi.org/10.1016/j.soildyn.2017.01.030.

Iai S, Tobita T and Nakahara T. (2005). Generalized scaling relations for dynamic centrifuge tests. Geotechnique, 55(5): 355–362.

Jamiolkowski, M., Ladd, C. C., Germaine, J. T., Lancellotta, R. (1985). New developments in field and laboratory testing of soils. Proc., XI ICSMFE, Vol. 1, A.A. Balkema, Rotterdam, Netherlands, 57–153.

Kim, J. H., Choo, Y. Y. W., Kim, D. J., Kim, D. S. (2016). Miniature cone tip resistance on sand in a centrifuge. Journal of Geotechnical and Geoenvironmental Engineering, 142(3), 04015090.

Kutter B.L., Manzari M.T., Zeghal M, Zhou Y.G., Armstrong R.J. (2015). Proposed outline for LEAP verification and validation processes. In: Iai Susumu, editor. Geotechnics for catastrophic flooding events, pp. 99-108.

Kutter, B. L., Carey, T. J., Hashimoto, T., Zeghal, M., Abdoun, T., Kokkali, P., et al. (2017). LEAP-GUW-2015 experiment specifications, results, and comparisons. Soil Dynamics and Earthquake Engineering, S0267726117304591.

Liu, K., Zhou, Y.G., She, Y., Meng, D., Xia, P., Huang, J.S., Yao, G., Chen, Y.M. (2018). Specifications and Results of Centrifuge Model Test at Zhejiang University for LEAP-UCD-2017.

Manzari M.T., Kutter B.L., Zeghal M, Iai S, Tobita T, Madabhushi S.P.G., Haigh S.K., Mejia L, Gutierrez D.A., Armstrong R.J. (2015). LEAP projects: concept and challenges. In: Proceedings of the fourth international conference on geotechnical engineering for disaster mitigation and rehabilitation (4th GEDMAR): 2014 Sept 16–18. Kyoto, Japan: Taylor and Francis.

TobitaT, Manzari M.T., Ozutsumi O, Ueda K, Uzuoka R, Iai S. (2015) Benchmark centrifuge tests and analyses of liquefaction-induced lateral spreading during earthquake. In: Iai Susumu, editor. Geotechnics for catastrophic flooding events, pp. 127-82.

White, D.J., Take, W.A. and Bolton, M.D. (2003). Soil deformation measurement using particle image velocimetry (PIV) and photogrammetry. Geotechnique, 53(7), pp.619-631.

Zhou, Y.G., Sun, Z.B., Chen, Y. M. (2017). Zhejiang University benchmark centrifuge test for LEAP-GWU-2015 and liquefaction responses of a sloping ground. Soil Dynamics and Earthquake Engineering, https://doi.org/10.1016/j.soildyn.2017.03.010.